NANO LETTERS

pubs.acs.org/NanoLett Letter

Non-Classical Euler Buckling and Brazier Instability in Cylindrical Liquid Droplets

Emery Hsu, Daeyeon Lee,* and Eli Sloutskin*

Cite This: *Nano Lett.* 2024, 24, 8717−8722 Read Online

ACCESS | Metrics & More | Article Recommendations | Supporting Information

ABSTRACT: Crystalline monolayers prevalent in nature and technology possess elusive elastic properties with important implications in fundamental physics, biology, and nanotechnology. Leveraging the recently discovered shape transitions of oil-in-water emulsion droplets, upon which these droplets adopt cylindrical shapes and elongate, we investigate the elastic characteristics of the crystalline monolayers covering their interfaces. To unravel the conditions governing Euler buckling and Brazier kink formation in these cylindrical tubular interfacial crystals, we strain the elongating cylindrical droplets within confining microfluidic wells. Our experiments unveil a nonclassical relation between the Young's modulus and the bending modulus of these crystals. Intriguingly, this relation varies with the radius of the cylindrical crystal, presenting a nonclassical mechanism for tuning of elasticity in nanotechnology applications.

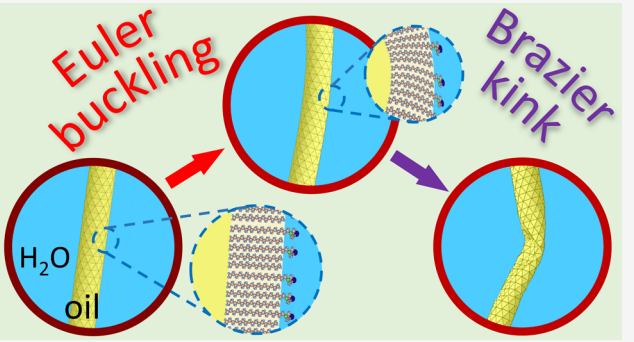

KEYWORDS: *interfacial freezing, two-dimensional crystal, elasticity, emulsion, self-faceting, self-shaping*

Classical theoretical models,[1,2] preclude the existence of true two-dimensional (2D) crystals, arguing that the long-range two-dimensional crystalline order is rendered untenable by thermal elastic vibrations. However, in the past few decades numerous experimental instances of 2D crystals have been identified, playing pivotal roles in various technological applications.[3−6] The current debate and interest center at whether the classical theories are incomplete in explaining the nature of these crystals,[7] or if the crystalline order in these crystals is not truly long-ranged.[8,9] Both scenarios have important implications for the elastic properties of the 2D crystals, suggesting deviations from the typical ones of classical bulk matter.[9−13] However, direct experimental 2D crystals' elasticity studies are challenging,[6,14−17] leading to a scarcity of results that hinders both fundamental understanding and practical applications.[11,12,18] Particularly challenging are the studies of 2D molecular crystals, self-assembling at liquid interfaces by adsorption from the bulk phase,[19] as such bulk-soluble crystals, possibly playing an important role in biology,[20,21] and promising for their potential technological applications,[22−24] evade conventional barrier compression methods. Moreover, many common 2D crystals are nonplanar, further challenging the exploration of their elastic properties.

We explore the elasticity of cylindrical tubule-shape 2D crystals, self-assembled at the interfaces of oil-in-water emulsion droplets (Figure 1a). By following the conditions for these crystals' Euler bending and Brazier kinking,[25] we extract the relation between the 2D Young's modulus Y_{2D} and the bending modulus κ of these tubule-forming molecular monolayer crystals. We reveal that the classical thin-plate $Y_{2D}(\kappa)$ relation[13,17,25,26] does not hold. Strikingly, the extracted moduli exhibit a strong dependence on the radius of the tubular crystal, r. We demonstrate that the observed apparent r − dependence may indicate that the spontaneous curvature radius of the studied 2D crystals is finite, with important consequences for liquid droplets' self-faceting transitions and beyond.[27]

Here-studied 2D crystals self-assemble at the interfaces of hexadecane $[CH_3(CH_2)_{14}CH_3]$ emulsion droplets, stabilized in water by the sodium octadecyl sulfate $[CH_3(CH_2)_{17}OSO_3Na$, 98% Thermo Scientific] surfactant. Upon cooling below the so-called "interfacial freezing" temperature T_s, the alkane and the surfactant molecules residing in the interfacial monolayer of these droplets adopt a fully extended, all-trans, conformation, with their axes orienting in-normal to the interface.[28,29] As for other similar alkane:surfactant combinations, the interfacial freezing is manifested by a dramatic change in the temperature slope of the interfacial tension, $\gamma(T)$: while a near-zero *negative* $d\gamma/dT$, typical for disordered liquid interfaces, is observed at $T > T_s$,

Received: May 5, 2024
Revised: July 2, 2024
Accepted: July 3, 2024
Published: July 8, 2024

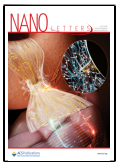

https://doi.org/10.1021/acs.nanolett.4c02075
Nano Lett. 2024, 24, 8717−8722

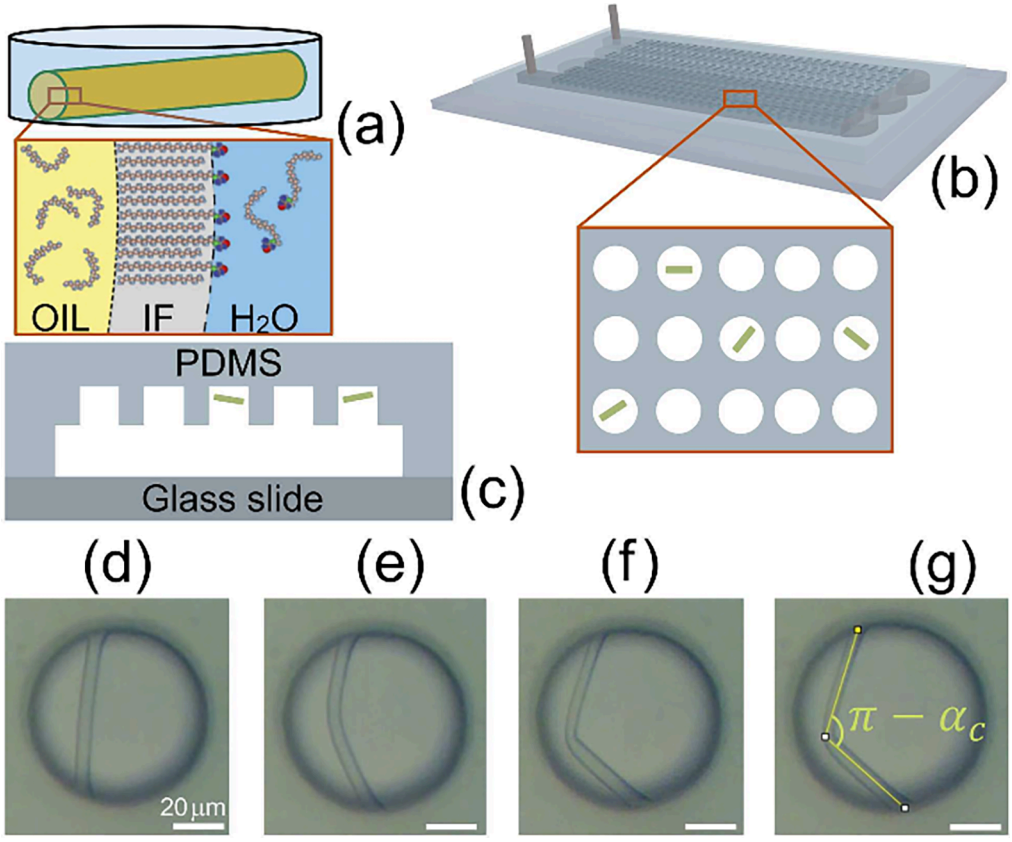

Figure 1. (a) Cylindrical liquid droplet of oil (hexadecane) in an aqueous sodium octadecyl sulfate surfactant solution. The cylindrical shape of the droplet is dictated by thermodynamic and elastic properties of the interfacially frozen (IF) monolayer crystal, covering the surface of the droplet[32] (see blown-up insert). The IF crystal is composed of a cocrystallized alkane:surfactant mixture.[23,32] (b) 3D view of the microfluidic device. Note the blown-up top-view of 15 wells inside the device. Cylindrical droplets are shown to reside in four of the wells. (c) A side view of our device, with the cylindrical droplets residing in two of the five wells shown. As the surface area of a droplet increases in the microwell, the droplet evolves from (d) a straight tubule to (e) a tubule undergoing Euler buckling and eventually to (f) a tubule exhibiting Brazier kink formation. Panel (g) demonstrates angle measurement at kink formation. The marked angle, $(\pi - \alpha_c)$, is complementary to the critical angle α_c, which is discussed in the text. Scale bar length in panels (d)-(g) is 20 μm.

the slope switches to a large *positive* value $C = d\gamma/dT \approx 0.8$ mN/m/K at $T < T_s$, where the interface is frozen.[22,28,30,31] Consequently, γ goes down on cooling below T_s, and vanishes at $T_{SE} = T_s - \gamma(T_s)/C$.

The dramatic reduction of γ in the vicinity of T_{SE}, enables the elastic energy of the interfacial crystal to dominate the shape of the liquid droplets, giving rise to droplet shape transformations.[29,32] Furthermore, on cooling to $T < T_{SE}$, droplets' interfaces transiently adopt a negative γ, which promotes further shape transformations with a dramatic increase in interfacial area.[29,32] While a different droplet self-shaping mechanism has been proposed in some early studies,[33,34] recent experimental evidence strongly supports the present scenario.[23,29,35,36] In the negative-γ regime, many droplets adopt a cylindrical shape,[32] with the length of the cylinder increasing as a function of time. This increase is accompanied by thinning of cylinder's cross section, warranting droplet's volume conservation. The 2D crystal, covering the surface of such a droplet, is rapidly restructuring: this crystal's destruction would raise γ to its near-T_s value of ≈5 mN/m, resulting in droplet's return to the spherical shape.[29] In previously studied *bulk* emulsion samples,[23,31,33,34] the increase in droplets' surface areas at $T < T_{SE}$, accompanied by surfactant adsorption from the aqueous bulk to the newly created interfacial areas, led to depletion in bulk surfactant concentration, increasing γ and prohibiting further surface area growth.

Here, we employ a microfluidic platform, where each oil droplet is confined to a separate well, and the aqueous solution within the wells is exchanged by flowing oil-free solution in a microchannel,[37] beneath the wells (see Figure 1b,c). Thus, no significant surfactant depletion takes place on the time scale of the experiment. Instead, the cylinder-shape droplets exhibit an accelerated growth until the cylinder's ends reach the side walls of the well. Further γ-driven growth applies a longitudinal stress onto the interfacially frozen 2D crystal, giving rise to cylindrical droplet's buckling, breaking the rotational symmetry about its long axis (Figure 1d,e). Initially, the buckling transition induces a global bending of the cylindrical droplet, as in the classical Euler's buckling instability, observed in slender columns succumbing to an excessive load.[26] However, upon further growth of the cylinder's length, which is accompanied by its cross section thinning, a local kink is formed, roughly in the middle of the cylinder's length. The bending focuses at the kink, with the rest of the cylinder straightening (Figure 1f). This kink formation, known as Brazier instability,[38] is followed by cylinder's folding and further elongation (Supplementary Video 1). At this stage, the droplet becomes too thin for its visualization with our current optical setup.

https://doi.org/10.1021/acs.nanolett.4c02075
Nano Lett. 2024, 24, 8717−8722

Our experimental observation that the buckling cylindrical droplets' lateral deviations are maximal near their center, monotonically decreasing toward the ends (i.e., first-mode buckling; Figure 1e) provides an important insight into the elastic properties of their 2D crystalline surfaces. While the critical load for Euler's buckling of a slender rod is always lower than the one for the rod's higher-mode bending,[26] cylindrical shells may, instead of the buckling, fail by wall wrinkling instabilities. A wrinkling instability does not involve any bending of the long axis of the cylinder: the walls fold on themselves, without breaking the rotation symmetry of the axis.[25] The observed long axis bending of our droplets indicates the absence of wrinkling instabilities and sets a constraint onto the values of the elastic parameters. In particular, while the critical strain for Euler-like overall buckling of a cylindrical tube of length L and radius r (with hinged edges) is $\epsilon_c^{(1)}=(\pi r/L)^2/2$, the critical strain for the lowest (i.e., second) mode of walls' wrinkling is estimated[25] as $\epsilon_c^{(2)} = 2r^{-1}\sqrt{\kappa/Y_{2D}}$. Using the classical elastic thin plate relation:[26]

$$Y_{2D} = 12\kappa(1-\nu^2)/t^2 \quad (1)$$

where t is the wall thickness and ν is the Poisson's ratio, the last expression is recast as[25] $\epsilon_c^{(2)} = r^{-1}t[3(1-\nu^2)]^{-1/2}$. The obtained $\epsilon_c^{(1)}$ and $\epsilon_c^{(2)}$ yield a necessary condition for the buckling to take place: $\epsilon_c^{(1)}<\epsilon_c^{(2)}$. If this condition is violated, the cylinder fails through wall wrinkling, with no buckling taking place. Since all the parameters in this condition, except for ν, are known, we use the buckling condition to set the bottom limit on the Poisson's ratio: $\nu > [1-(4/3)(tL^2/\pi^2r^3)^2]^{1/2}$. The length of the cylindrical droplets at the buckling transition is equal to the diameter of the well, $L = 70\ \mu$m. Interfacial crystal's thickness is[28,29,36] $t \approx 2$ nm. The radius of the thickest cylinders observed to buckle is $r = 2.9\ \mu$m. Strikingly, we obtain an anomalous $\nu > 0.999$, far beyond the range of ν allowed in classical stable elastic matter.[26] The unphysical limit obtained for ν, indicates that the classical elastic thin plate relation fails for the interfacially frozen crystalline monolayers, in agreement with several previous studies of 2D solids.[13,17,32,39]

To obtain a further insight into our cylindrical crystals' elasticity, we measure the critical bending angle α_c, at which the Brazier instability takes place, forming a localized kink in the middle of the cylindrical droplet (Figure 1g). The experimental α_c exhibits a monotonic increase with the cylinder radius r (Figure 2a). Thus, the thinnest droplets bend the least prior to their kinking, while the thicker droplets can bend a lot, without the Brazier instability setting in. Strikingly, an opposite behavior has been predicted and reproduced by computer simulations, in carbon nanotubes: the critical curvature of the nanotubes was demonstrated to scale as r^{-2}, so that the thinnest nanotubes can bend much stronger than the thicker ones, prior to kink formation.[25] Note that there is a fundamental difference between the tubular interfacially frozen crystals and the carbon nanotubes. While the ends of the carbon nanotubes can either be open or closed, and the internal volume of a nanotube may change freely, our cylindrical droplets are fully covered with an interfacially frozen crystal. The bulk of our droplets is an incompressible oil phase, so that the volume of each individual droplet is conserved.

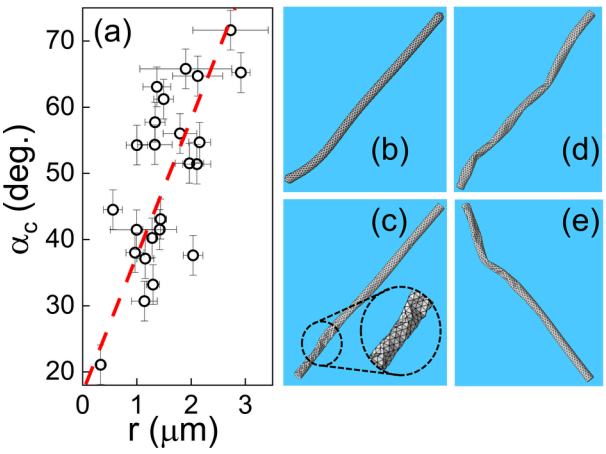

Figure 2. (a) The experimental critical angle α_c for Brazier kink formation *increases* with the cylindrical droplet's radius r, contrasting with the kink formation conditions in carbon nanotubes. The error bars represent the estimated accuracy of the measurement of α_c and r. (b) Computer simulations reproduce Euler buckling when the Föppl-von Kármán (FvK) number is in the range $10 \lesssim FvK \lesssim 5\times10^3$, while crumpled shapes (c) are exhibited at higher FvK, and wall folding supersedes buckling at lower FvK (not shown). Brazier kink formation, observed in the same computer simulations at higher strains, may either (d) occur simultaneously at several different spots along the droplet, or (e) take place at an individual spot, as in the experiments.

Volume conservation limits the accessible conformations of our cylinders.

To model cylindrical droplets' buckling and kinking subject to the constraint of volume conservation, we employ numerical Surface Evolver simulations.[40] Notably, our present approach allows both dimensionless elastic parameters: the Föppl-von Kármán number $FvK = Yr^2/\kappa$ and the Poisson's ratio, ν, to be varied. It is therefore superior to most previous simulations of unconstrained droplet shape transformations,[22,23,29,32] where a triangular Hookean springs' network was employed, arbitrarily fixing $\nu = 1/3$. Since the value of the critical strain at the onset of Euler's instability is highly noise-sensitive, we only employ the simulations to test the overall appearance of the buckled shapes, for a qualitative comparison with the shapes of the experimental droplets. Remarkably, when the volume conservation constraint is employed, the buckled shape exhibits a nontrivial dependence on κ and ν. In particular, at the intermediate values of the bending modulus: $10 \lesssim FvK \lesssim 5\times10^3$, the cylinder exhibits the classical Euler buckling, with its walls undergoing no crumpling or wrinkling, for any value of ν (Figure 2(b)). For larger FvK, the shape depends on the Poisson's ratio: for small and negative ν, the surfaces of the droplets are relatively smooth, but the tendency to crumpling and wrinkling increases for larger ν values (Figure 2(c)). Finally, for very small FvK, no buckling takes place whatsoever. Instead, we see cylinders' walls folding on themselves (almost) without breaking the symmetry of rotation about the long axis of the cylinder.

To gain a comprehensive understanding of instabilities within our system, we systematically investigate a broad spectrum of (FvK,ν) combinations. For each combination, we measure the integral of squared mean curvature over the (distorted-) cylindrical shape, at the onset of shape instability. Smaller integral values are obtained for smoother and less-crumpled shapes, allowing the full spectrum to be captured by

https://doi.org/10.1021/acs.nanolett.4c02075
Nano Lett. 2024, 24, 8717−8722

a single plot (Figure 3). Importantly, taken that the experimental cylindrical droplets are (a) optically smooth;

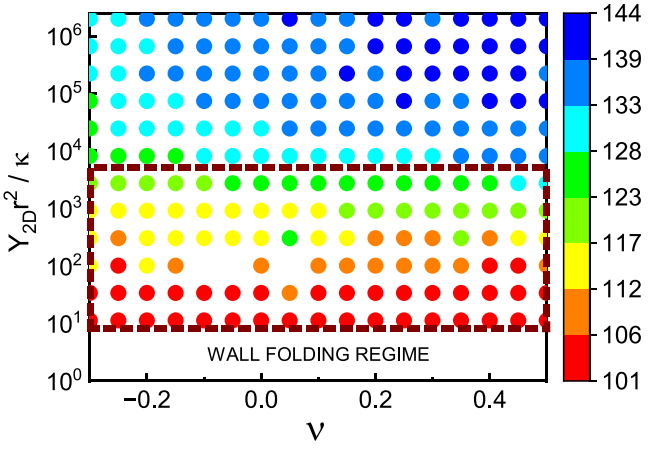

Figure 3. Squared mean curvature, integrated over the simulated droplet shape, at the onset of Euler buckling instability, is encoded in the color map, for a wide range of Föppl-von Kármán values ($Y_{2D}r^2/\kappa$) and Poisson's ratios (ν). Large squared mean curvature values corresponds to shapes exhibiting crumpled and rough surfaces. Note, while a significant ν-dependence is observed at high-FvK, the dependence is much weaker at low FvK. The experimentally relevant regime of intermediate FvK is marked by dashes.

and (b) fail through Euler's buckling, with no visible crumpling, we conclude that the experimentally relevant range of FvK is from ~10 to ~5×10^3 (marked by brown dashes in Figure 3). In this range of FvK values, the dependence on ν is rather weak, suggesting that a simpler analytical estimate may be employed to describe the experimental $\alpha_c(r)$ variation at the onset of Brazier instability.

To obtain an analytical estimate for the Brazier instability conditions, we note that during kinking, (only) one side of the tube is compressed and buckles (see the simulated shapes in Figure 2(d,e)). As in the studies of carbon nanotubes,[25] we assume that the buckling occurs when the local strain $\epsilon = Kr$, where K is the local curvature, is approximately equal to $\epsilon_c^{(2)}$. Consequently, $\alpha_c = (2L/r^2)\sqrt{\kappa/Y_{2D}}$, and we employ the experimental $\alpha_c(r)$ to obtain an estimate for $\sqrt{\kappa/Y_{2D}}$ of the interfacial monolayer crystal, covering the surfaces of our cylindrical droplets. Importantly, this derivation does not rely on the classical thin plate relation (eq 1), which otherwise leads to nonphysical ν value, as for the Euler's buckling above. Remarkably, the obtained $\sqrt{\kappa/Y_{2D}}$ exhibits a significant r-dependence, as demonstrated in Figure 4(a). Clearly, these results contrast with the classical solid matter elasticity, where the moduli are r-independent. We note that the observed r-dependence appears almost perfectly linear, when plotted on a log–log scale (Figure 4(b)). Thus, we fit to it a power-law dependence: $\sqrt{\kappa/Y_{2D}} = (4.4 \pm 0.9) \times 10^{-3} r^{2.42\pm0.09}$ μm, where r is in μm (Figure 4(b), red line). Note the excellent match between this fit and the experimental data. We also note that for $r \approx 32$ nm, this fit matches the previously estimated limit: $\sqrt{\kappa/Y_{2D}} < 2.6 \times 10^{-3}$ μm, based on the observation that droplets of radius ≈32 nm exhibit a sphere-to-icosahedron shape transition.[29]

The observed anomaly of the elastic moduli r-dependence is further supported by returning to analysis of Euler buckling

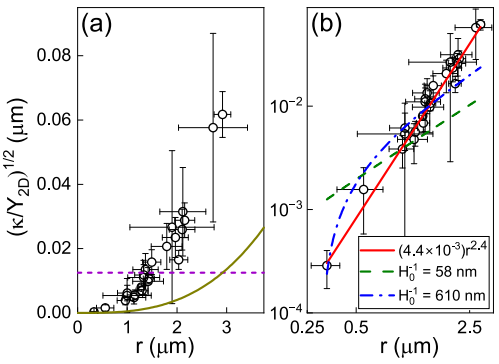

Figure 4. $\sqrt{\kappa/Y_{2D}}$ ratio, obtained from the experimental critical angles α_c corresponding to the onset of Brazier kink instability (see Figure 2(a)), are shown (a) on a linear and (b) on a log–log scale (scatter). The bottom limit, below which no Euler-like buckling may take place, is shown in (a), with the r-dependence of the moduli either excluded (short purple dashes) or allowed (solid dark yellow curve). Since buckling is observed for all droplets studied, $\sqrt{\kappa/Y_{2D}}$ values falling below the purple dashes invalidate this limit, suggesting that the r-dependence of the moduli cannot be excluded. Note that $\sqrt{\kappa/Y_{2D}}$ fall above the *solid* curve, in agreement with the experimental observations. In (b), the data are overlaid by a phenomenological power-law fit (solid red line). Fits assuming a nonzero spontaneous curvature H_0 of the interfacial crystal are shown as well. See legend for the corresponding spontaneous curvature radii. The error bars are due to the finite accuracy of our experimental r.

conditions. As discussed above, for the Euler-like buckling of our cylindrical droplets to avoid being preceded by higher-mode instabilities, the corresponding strains should fulfill $\epsilon_c^{(1)} < \epsilon_c^{(2)}$. With the classical thin plate relation (eq 1) avoided, we obtain $\sqrt{\kappa/Y_{2D}} > (\pi/2L)^2 r^3$. If $\sqrt{\kappa/Y_{2D}}$ is r-independent, the present inequality implies that $\sqrt{\kappa/Y_{2D}} \gtrsim 1.3 \times 10^{-2}$ μm, since we observe the buckling transition to take place for r values at least up to 2.9 μm. This condition, shown in short purple dashes in Figure 4(a), is violated by the experimental data for $r \lesssim 1.45$ μm. However, if moduli variation is allowed, a much weaker condition on κ/Y_{2D} sets in. This weaker condition is fulfilled by the experimental data: the $\sqrt{\kappa/Y_{2D}}$ values fall above the limit on Euler-like buckling (cf. scatter and dark yellow curve in Figure 4(a)), in line with the experimental observation that all the cylindrical droplets undergo buckling.

While our present data do not allow the origin of the observed r-dependence to be unequivocally determined, we suggest here several possible mechanisms for this unexpected observation. First, the small-r cylindrical shapes have a lower surface area. Thus, the number of structural defects (coupled to possible fluctuations of Gaussian curvature[41]) and surface-adsorbed impurities is smaller, so that the structure of the interfacial crystal is closer to being perfect and its Y_{2D} is higher. Another possibility is that the unscreened electrostatic fields due to the charged head groups of the interfacial surfactants penetrate through the bulk oil of the small-r droplets,[42] so that the ensuing electrostatic contribution modifies the elastic moduli. The third possibility is that the interfacial crystal exhibits a nonzero spontaneous curvature, as also suggested by a recent theoretical model of self-faceting.[27] Note that the interfacial crystal is formed by the cocrystallization of alkane and surfactant molecules, with the effective cross section of the

https://doi.org/10.1021/acs.nanolett.4c02075
Nano Lett. 2024, 24, 8717−8722

surfactant's headgroup[43] (≈30 Å^2) far exceeding the cross section of these molecules' alkyl tails (≈20 Å^2). Furthermore, since the anionic headgroup may be ionized in water, with the adjacent head groups repelling by Coulomb forces, the effective cross section of the headgroup may significantly exceed its steric dimensions. The difference between the cross sections of the heads and the tails may possibly give rise to a nonzero spontaneous curvature,[44] H_0. However, its value is difficult to predict from the first-principles, as it depends on both the relative interfacial concentration of the alkanes and the surfactants, and the surfactant head groups' ionization ratio.[43] Qualitatively, we observe that the introduction of a positive H_0 into our Surface Evolver simulations increases the tendency of thinner cylinders to buckle and is therefore expected to promote their kink instability. Thus, on a qualitative level, $H_0 > 0$ may be responsible for the observed r-variation of the moduli.

To additionally support the hypothesis that the r-variation of the moduli stems from nonzero H_0, we note that the bending energy (per unit area) term appearing in the Hamiltonian[27] is $2\tilde{\kappa}(H - H_0)^2 = 2\tilde{\kappa}H^2 - 4HH_0\tilde{\kappa} + 2\tilde{\kappa}H_0^2$, where $\tilde{\kappa}$ is the bending modulus and H is the mean curvature. Neglecting spontaneous curvature, amounts to replacing the bending energy term by $2\kappa H^2$. The bending modulus κ, appearing in H_0-neglecting formalism, is related to the bending modulus $\tilde{\kappa}$ of the H_0-preserving formalism as $\kappa = \tilde{\kappa} - 2(H_0/H)\tilde{\kappa} + \tilde{\kappa}(H_0/H)^2$. In a cylinder, $H = 1/(2r)$, so that $\kappa = \tilde{\kappa}(1 - 4H_0r + 4H_0^2r^2)$. Thus, the neglected spontaneous curvature may give rise to an r-dependent κ, even if the true bending modulus, $\tilde{\kappa}$, is constant. To obtain an estimate for H_0, we fit our $\sqrt{\kappa/Y_{2D}}$ data by $\sqrt{\tilde{\kappa}/Y_{2D}}[1 - 4H_0r + 4H_0^2r^2]^{1/2}$. Remarkably, the correct overall trend is reproduced with H_0^{-1} fixed to 58 nm, as estimated previously by a theoretical model of self-faceting, for an emulsion stabilized by a cationic (octadecyltrimethylammonium bromide) surfactant[27] (green dashes). Note that this fit is obtained with only one tunable parameter. An even better match is obtained if H_0 is allowed to vary. Since an *anionic* surfactant, with a different headgroup, is employed in the present work, the H_0 value may be completely different from the one estimated in previous studies.[27] Indeed, we obtain $H_0^{-1} \approx 610$ nm, indicating that the spontaneous curvature in our system is smaller, in line with the smaller mismatch between the headgroup and the tail cross sections in sodium octadecyl sulfate, compared to octadecyltrimethylammonium bromide. Future systematic studies of buckling and kink formation in cylinder-shape emulsion droplets stabilized by a wide range of surfactants, may allow the hypothesized mechanism of moduli r-dependence to be verified.

Conclusions. We have demonstrated, that the cylinder-shape interfacially frozen emulsion droplets confined within a microwell, undergo Euler-like buckling and Brazier kink formation instabilities during their spontaneous elongation. We have leveraged these confinement-induced shape transformations to probe the elastic properties of cylindrical monolayer crystals, covering the surfaces of these droplets. We observe, that the classical thin elastic plate relation between bending modulus and Young's modulus is invalid for these 2D crystals, indicating that κ and Y_{2D} can in principle, be independently tuned in these systems, providing unique flexibility for material engineering, which is not available for classical solids. Furthermore, we demonstrate that the ratio between these moduli exhibits an anomalous dependence on droplet size. We hypothesize that the origin of this dependence may either be the higher quality structure of the smallest interfacial crystals, the unscreened electrostatic field penetrating through the bulk of the droplet, or the finite spontaneous curvature of the interfacial crystal. Future studies, involving detailed atomic-resolution simulation of interfacially frozen crystals, may allow the spontaneous curvature value to be obtained from the first-principles, testing the proposed scenarios and providing a deeper understanding of droplets' self-faceting transitions and free cylinders' elongation dynamics.

■ ASSOCIATED CONTENT

Supporting Information

The Supporting Information is available free of charge at https://pubs.acs.org/doi/10.1021/acs.nanolett.4c02075.

Further details of the samples, measurements, and computer simulations (PDF)

Video of an elongating cylindrical droplet, confined in a micrfluidic well. The droplet exhibits Euler buckling and Brazier instability (AVI)

■ AUTHOR INFORMATION

Corresponding Authors

Daeyeon Lee − *Department of Chemical and Biomolecular Engineering, University of Pennsylvania, Philadelphia, Pennsylvania 19104, United States;* orcid.org/0000-0001-6679-290X; Email: daeyeon@seas.upenn.edu

Eli Sloutskin − *Physics Department & Institute of Nanotechnology and Advanced Materials, Bar-Ilan University, Ramat Gan 529002, Israel;* orcid.org/0000-0002-7109-6893; Email: eli.sloutskin@biu.ac.il

Author

Emery Hsu − *Department of Chemical and Biomolecular Engineering, University of Pennsylvania, Philadelphia, Pennsylvania 19104, United States*

Complete contact information is available at: https://pubs.acs.org/10.1021/acs.nanolett.4c02075

Notes

The authors declare no competing financial interest.

■ ACKNOWLEDGMENTS

This research was supported by Grant No. 2110611 from the United States National Science Foundation (NSF) and the United States-Israel Binational Science Foundation (BSF). We thank Paradorn Rummaneethorn and Hyejoong Jeong for helpful discussions and the optimization of the microfluidic device design and fabrication protocol. We also thank Alexander V. Butenko and Moshe Deutsch for fruitful discussions.

■ REFERENCES

(1) Peierls, R. E. Quelques Propriétés Typiques des Corpses Solides. *Ann. Inst. H. Poincaré* **1935**, *5*, 177−222.

(2) Mermin, N. D. Crystalline Order in Two Dimensions. *Phys. Rev.* **1968**, *176*, 250−254.

(3) Novoselov, K. S.; Geim, A. K.; Morozov, S. V.; Jiang, D.; Zhang, Y.; Dubonos, S. V.; Grigorieva, I. V.; Firsov, A. A. Electric Field Effect in Atomically Thin Carbon Films. *Science* **2004**, *306*, 666−669.
(4) Zhang, X.; Xie, Y. Recent Advances in Free-Standing Two-Dimensional Crystals with Atomic Thickness: Design, Assembly and Transfer Strategies. *Chem. Soc. Rev.* **2013**, *42*, 8187−8199.
(5) Zhang, Z.; Forti, S.; Meng, W.; Pezzini, S.; Hu, Z.; Coletti, C.; Wang, X.; Liu, K. Growth and Applications of Two-Dimensional Single Crystals. *2D Mater.* **2023**, *10*, 032001.
(6) Swinkels, P. J. M.; Gong, Z.; Sacanna, S.; Noya, E. G.; Schall, P. Visualizing Defect Dynamics by Assembling the Colloidal Graphene Lattice. *Nat. Commun.* **2023**, *14*, 1524.
(7) O'Hare, A.; Kusmartsev, F. V.; Kugel, K. I. A Stable 'Flat' Form of Two-Dimensional Crystals: Could Graphene, Silicene, Germanene be Minigap Semiconductors? *Nano Lett.* **2012**, *12*, 1045−1052.
(8) Nelson, D. R.; Halperin, B. I. Dislocation-Mediated Melting in Two Dimensions. *Phys. Rev. B* **1979**, *19*, 2457−2484.
(9) Kosterlitz, J. M. Kosterlitz−Thouless Physics: a Review of Key Issues. *Rep. Prog. Phys.* **2016**, *79*, 026001.
(10) Li, R.; Shao, Q.; Gao, E.; Liu, Z. Elastic Anisotropy Measure for Two-Dimensional Crystals. *Extreme Mechanics Letters* **2020**, *34*, 100615.
(11) Zanghellini, J.; Keim, P.; von Grünberg, H. H. The Softening of Two-Dimensional Colloidal Crystals. *J. Phys.: Condens. Matter* **2005**, *17*, S3579.
(12) Gasser, U.; Eisenmann, C.; Maret, G.; Keim, P. Melting of Crystals in Two Dimensions. *ChemPhysChem* **2010**, *11*, 963−970.
(13) Quemeneur, F.; Quilliet, C.; Faivre, M.; Viallat, A.; Pépin-Donat, B. Gel Phase Vesicles Buckle into Specific Shapes. *Phys. Rev. Lett.* **2012**, *108*, 108303.
(14) Lee, C.; Wei, X.; Kysar, J. W.; Hone, J. Measurement of the Elastic Properties and Intrinsic Strength of Monolayer Graphene. *Science* **2008**, *321*, 385−388.
(15) Cao, K.; Feng, S.; Han, Y.; Gao, L.; Hue Ly, T.; Xu, Z.; Lu, Y. Elastic Straining of Free-Standing Monolayer Graphene. *Nat. Commun.* **2020**, *11*, 284.
(16) Li, Y.; Yu, C.; Gan, Y.; Jiang, P.; Yu, J.; Ou, Y.; Zou, D.-F.; Huang, C.; Wang, J.; Jia, T.; Luo, Q.; Yu, X.-F.; Zhao, H.; Gao, C.-F.; Li, J. Mapping the Elastic Properties of Two-Dimensional MoS_2 via Bimodal Atomic Force Microscopy and Finite Element Simulation. *NPJ. Comput. Mater.* **2018**, *4*, 49.
(17) Toor, A.; Forth, J.; Bochner de Araujo, S.; Merola, M. C.; Jiang, Y.; Liu, X.; Chai, Y.; Hou, H.; Ashby, P. D.; Fuller, G. G.; Russell, T. P. Mechanical Properties of Solidifying Assemblies of Nanoparticle Surfactants at the Oil−Water Interface. *Langmuir* **2019**, *35*, 13340−13350.
(18) Cohen, A. E.; Mahadevan, L. Kinks, rings, and rackets in filamentous structures. *Proc. Natl. Acad. Sci. U. S. A.* **2003**, *100*, 12141−12146.
(19) Lang, P. Surface Induced Ordering Effects in Soft Condensed Matter Systems. *J. Phys.: Condens. Matter* **2004**, *16*, R699.
(20) Kang, L.; Lubensky, T. C. *Chiral Twist Drives Raft Formation and Organization in Membranes Composed of Rod-Like Particles*. Proceedings of the National Academy of Sciences 2017, *114*, E19−E27.
(21) Sezgin, E.; Levental, I.; Mayor, S.; Eggeling, C. The Mystery of Membrane Organization: Composition, Regulation and Roles of Lipid Rafts. *Nat. Rev. Mol. Cell Biol.* **2017**, *18*, 361−374.
(22) Das, S.; Butenko, A. V.; Mastai, Y.; Deutsch, M.; Sloutskin, E. Topology-Driven Surface Patterning of Liquid Spheres. *Nat. Phys.* **2022**, *18*, 1177−1180.
(23) Marin, O.; Tkachev, M.; Sloutskin, E.; Deutsch, M. Polyhedral Liquid Droplets: Recent Advances in Elucidation and Application. *Curr. Opin. Colloid Interface Sci.* **2020**, *49*, 107−117.
(24) Zhao, Y.; An, L.; Fang, J. Buckling of Lipid Tubules in Shrinking Liquid Droplets. *Nano Lett.* **2007**, *7*, 1360−1363.
(25) Yakobson, B. I.; Brabec, C. J.; Bernholc, J. Nanomechanics of Carbon Tubes: Instabilities beyond Linear Response. *Phys. Rev. Lett.* **1996**, *76*, 2511−2514.
(26) Landau, L. D.; Lifshitz, E. M. *Elasticity Theory*; Pergamon: Oxford, 1986.
(27) García-Aguilar, I.; Fonda, P.; Sloutskin, E.; Giomi, L. Faceting and Flattening of Emulsion Droplets: A Mechanical Model. *Phys. Rev. Lett.* **2021**, *126*, 038001.
(28) Tamam, L.; Pontoni, D.; Sapir, Z.; Yefet, S.; Sloutskin, E.; Ocko, B. M.; Reichert, H.; Deutsch, M. Modification of Deeply Buried Hydrophobic Interfaces by Ionic Surfactants. *Proc. Natl. Acad. Sci. U.S.A.* **2011**, *108*, 5522−5525.
(29) Guttman, S.; Kesselman, E.; Jacob, A.; Marin, O.; Danino, D.; Deutsch, M.; Sloutskin, E. Nanostructures, Faceting, and Splitting in Nanoliter to Yoctoliter Liquid Droplets. *Nano Lett.* **2019**, *19*, 3161−3168.
(30) Sloutskin, E.; Sapir, Z.; Bain, C. D.; Lei, Q.; Wilkinson, K. M.; Tamam, L.; Deutsch, M.; Ocko, B. M. Wetting, Mixing, and Phase Transitions in Langmuir-Gibbs Films. *Phys. Rev. Lett.* **2007**, *99*, 136102.
(31) Sloutskin, E.; Bain, C. D.; Ocko, B. M.; Deutsch, M. Surface Freezing of Chain Molecules at the Liquid-Liquid and Liquid-Air Interfaces. *Faraday Discuss.* **2005**, *129*, 339−352.
(32) Guttman, S.; Sapir, Z.; Schultz, M.; Butenko, A. V.; Ocko, B. M.; Deutsch, M.; Sloutskin, E. How Faceted Liquid Droplets Grow Tails. *Proc. Natl. Acad. Sci. U.S.A.* **2016**, *113*, 493−496.
(33) Denkov, N.; Tcholakova, S.; Lesov, I.; Cholakova, D.; Smoukov, S. K. Self-Shaping of Oil Droplets via the Formation of Intermediate Rotator Phases upon Cooling. *Nature* **2015**, *528*, 392−395.
(34) Cholakova, D.; Denkov, N.; Tcholakova, S.; Lesov, I.; Smoukov, S. K. Control of Drop Shape Transformations in Cooled Emulsions. *Adv. Coll. Interface Sci.* **2016**, *235*, 90−107.
(35) Garcia-Aguilar, I.; Atkins, A.; Fonda, P.; Sloutskin, E.; Giomi, L. Reply. *Phys. Rev. Lett.* **2021**, *126*, 259802.
(36) Hacmon, S.; Liber, S. R.; Shool, L.; Butenko, A. V.; Atkins, A.; Sloutskin, E. "Magic Numbers" in Self-Faceting of Alcohol-Doped Emulsion Droplets. *Small* **2023**, *19*, 2301637.
(37) Seo, H.; Lee, H. Recent Developments in Microfluidic Synthesis of Artificial Cell-Like Polymersomes and Liposomes for Functional Bioreactors. *Biomicrofluidics* **2021**, *15*, 021301.
(38) Qiu, L.; Hutchinson, J. W.; Amir, A. Bending Instability of Rod-Shaped Bacteria. *Phys. Rev. Lett.* **2022**, *128*, 058101.
(39) Guttman, S.; Sapir, Z.; Ocko, B. M.; Deutsch, M.; Sloutskin, E. Temperature-Tuned Faceting and Shape-Changes in Liquid Alkane Droplets. *Langmuir* **2017**, *33*, 1305−1314.
(40) Brakke, K. A. The Surface Evolver. *Exp. Math.* **1992**, *1*, 141−165.
(41) Klebes, J.; Clegg, P.; Evans, R. M. L. Effects of Orientational Order on Modulated Cylindrical Interfaces. *Phys. Rev. E* **2022**, *105*, 064802.
(42) Zdrali, E.; Chen, Y.; Okur, H. I.; Wilkins, D. M.; Roke, S. The Molecular Mechanism of Nanodroplet Stability. *ACS Nano* **2017**, *11*, 12111−12120.
(43) Kralchevsky, P. A.; Danov, K. D.; Kolev, V. L.; Broze, G.; Mehreteab, A. Effect of Nonionic Admixtures on the Adsorption of Ionic Surfactants at Fluid Interfaces. 1. Sodium Dodecyl Sulfate and Dodecanol. *Langmuir* **2003**, *19*, 5004−5018.
(44) Israelachvili, J. N. *Intermolecular and surface forces*; Academic Press: London, 2010.

https://doi.org/10.1021/acs.nanolett.4c02075
Nano Lett. 2024, 24, 8717−8722